IEEE Access
Multidisciplinary | Rapid Review | Open Access Journal

Received March 11, 2021, accepted April 1, 2021, date of publication April 8, 2021, date of current version April 16, 2021.

Digital Object Identifier 10.1109/ACCESS.2021.3071793

Portable Optical Coherence Elastography System With Flexible and Phase Stable Common Path Optical Fiber Probe

ASHA PARMAR[1,2], GARGI SHARMA[1], SHIVANI SHARMA[1,2], AND KANWARPAL SINGH[1,2]
[1]Max Planck Institute for the Science of Light, 91058 Erlangen, Germany
[2]Department of Physics, Friedrich-Alexander Universität Erlangen-Nürnberg, 91058 Erlangen, Germany

Corresponding author: Kanwarpal Singh (kanwarpal.singh@mpl.mpg.de)

ABSTRACT Biomechanical properties drive the functioning of cells and tissue. Measurement of such properties in the clinic is quite challenging, however. Optical coherence elastography is an emerging technique in this field that can measure the biomechanical properties of the tissue. Unfortunately, such systems have been limited to benchtop configuration with limited clinical applications. A truly portable system with a flexible probe that could probe different sample sites with ease is still missing. In this work, we report a portable optical coherence elastography system based on a flexible common path optical fiber probe. The common path approach allows us to reduce the undesired phase noise in the system by an order of magnitude less than the standard non-common path systems. The flexible catheter makes it possible to probe different parts of the body with ease. Being portable, our system can be easily transported to and from the clinic. We tested the efficacy of the system by measuring the mechanical properties of the agar-based tissue phantoms. We also measured the mechanical properties (Young's Modulus) of the human skin at different sites. The measured values for the agar phantom and the skin were found to be comparable with the previously reported studies. Ultra-high phase stability and flexibility of the probe along with the portability of the whole system makes an ideal combination for the faster clinical adoption of the optical coherence elastography technique.

INDEX TERMS Elastography, medical diagnostic imaging, biomedical optical imaging.

I. INTRODUCTION

Biomechanical properties play an important role in the regulation of cellular functions within biological tissue. For instance, some cancer cell types are less stiffer than normal cells [1] and this information can be used as a diagnostic marker to differentiate cancerous cells from normal ones. Tissue elasticity is routinely used to determine breast cancer tissue margins during intraoperative breast cancer surgery [2], [3]. Similarly, in dermatology, skin elasticity has been used to diagnose systemic sclerosis [4]–[6]. Therefore, the measurement of the mechanical properties of the cells and the tissues have great clinical significance. The mechanical properties of tissues can be quantified by measuring parameters such as Young's modulus, bulk modulus, and shear modulus. However, in vivo measurement of the biomechanical properties of the tissues within clinical settings has been challenging because of the unavailability of compact portable measurement devices.

In current clinical settings, the Rodnan skin score (mRSS), based on skin palpation is still the most widely used method to determine the mechanical properties of skin [7]. However, the quantification and reliability of the mRSS score are highly dependent on the clinician's experience [8]. To address this issue in clinical praxis, several other methods such as Atomic-Force Microscopy (AFM) [9]–[11], Magnetic Resonance Elastography (MRE) [12], Ultrasound Elastography (USE) [13], Brillouin Scattering Microscopy (BSM) [14], and Optical Coherence Elastography (OCE) [15], [16] have been developed. These available techniques provide images, known as elastograms, by mapping the elastic properties of the tissue.

AFM provides stiffness maps at a subcellular level, however, it suffers from the drawback of slow throughput which restricts it from quickly analyzing the tissue mechanical properties over a large surface area. MRE is a non-invasive

The associate editor coordinating the review of this manuscript and approving it for publication was Xiahai Zhuang.

imaging technique that is based on the principle of the Magnetic Resonance Imaging technique. This technique measures the stiffness of the tissue by calculating the displacement in the tissue caused by the shear waves. USE detects tissue displacement by applying stress on the tissue using ultrasound waves. BSM is a non-destructive and label-free imaging technique to measure the elastic properties of the tissue in 3D. However, because of the long acquisition time of several minutes for 3D measurements, BSM has limited applications in the clinic. Recently, the use of stimulated Brillouin scattering has been proposed to reduce the acquisition time to ∼1 min for 2D measurements [17], but the requirement of two counter-propagating light beams inside the sample makes it unsuitable for the in-vivo measurements.

Optical coherence tomography (OCT) is a micron and submicron level imaging technique that is based on optical interferometry. This technique has better axial and lateral resolution with higher sensitivity than MRI and ultrasound imaging. OCT has been applied in a wide range of applications such as; ophthalmology [18], dermatology [19], oncology [20], cardiology [21], and cell mechanics [22]. OCE is an extension of OCT which is capable of measuring the mechanical properties of the biological samples. Initially, OCE was based on time-domain OCT. Low signal-to-noise ratio (SNR) and unstable phase measurements because of the long acquisition time for the time-domain-based OCE systems hindered their adoption in the clinic. The OCE was revived after the introduction of Fourier-domain OCT which offered better SNR and reduced acquisition time compared to the time-domain OCT systems [23].

Most of the Fourier domain OCE systems are still Michelson-interferometry based. Such systems measure the displacements in the tissue caused by some external stimulus against a fixed reference surface. In Michelson-interferometry-based system, measured displacement has additional noise because of the mechanical vibrations present between the reference arm and the sample arm. Such mechanical vibrations change the optical path difference between the two arms of the interferometer and appear as noise. The minimum measurable displacement in the tissue in such systems is thus limited by the undesirable optical path difference (OPD) change. The undesirable OPD change in the two arms of the interferometer can be minimized using a common path approach where the reference and the sample signal travel approximately the same optical path within the system. Fiber-based common path probes have been reported previously [24]–[30] and used for the imaging of tissue such as coronary artery [28], eye [31], [32], esophagus [29], etc. Owing to their superior phase measurement abilities, common path probes have also been used for angiographic applications [33], [34].

The potential of the common path approach has also been realized for the optical coherence elastography applications and benchtop [35]–[37] as well as fiber-based [38]–[41] common-path OCE systems have been reported. In clinical settings, fiber-based common path probes for elastography are preferred over their free space counterparts because of their lightweight and ease of handling.

OCE systems can be further classified into two categories; static/quasi-static and dynamic. Static/quasi-static based OCE systems provide better spatial resolution compared to dynamic OCE methods but these systems need careful calibration in order to quantify the results. Dynamic OCE systems using surface acoustic waves (SAW) are much simpler to operate as these systems require only a way to excite the SAW into the sample and a way to measure the speed of the SAW into the sample. The SAW can be excited using simple mechanisms such as piezo transducer [42], air puff [43], acoustic radiation force [44], etc., and the speed of the SAW can be measured using an OCT system.

The previous SAW-based OCE systems have focused on the scanning of the measurement beam over the sample in order to generate the tissue elastograms which leads to increased system complexity. However, for applications such as systemic sclerosis [4], [5], clinicians only need a reliable and repeatable number to quantify the skin elasticity; something similar to skin palpation which is still the standard diagnostic method. For such applications, there is no need to scan the measurement beam over the sample and only one measurement point would suffice. This however would allow the development of much simpler fiber probes and compact OCE systems which are more relevant to the clinical settings.

In this paper, we present a fiber-based common-path flexible OCE probe approach. We demonstrate a portable and handheld common path probe OCE system that can be easily transported to and from the clinic. Our flexible probe can be placed directly at the measurement site for the measurement of the tissue elastic properties. Unlike previously reported common path probes-based OCE systems, which have relied on the compression method [38]–[41], we report a common path probe that is compatible with the simpler SAW method of OCE.

II. MATERIALS AND METHODS

The schematic diagram of our system is shown in Figure 1. The system is based on a commercially available swept-source OCT engine (Axsun Technologies, USA). The OCT system has a central wavelength of 1310 nm, a bandwidth of 130 nm, and a repetition rate of 12.5 kHz. The output power of the laser source is 24 mW. In addition to the illumination unit, the system comes with components for the acquisition and processing of the data. Two photodiodes (D1, D2) capable of balanced detection are connected to a data acquisition card (DAQ), and a field-programmable gate array (FPGA). OCT data is processed on the integrated FPGA module which includes applying Hanning window on the acquired spectrum for side lob suppression, the wavelength to k-space linearization using the Mach Zender interferometer clock signal, and performing FFT on the windowed data. The FFT data is transferred to the host computer over the Ethernet cable. The host computer is composed of a processing unit

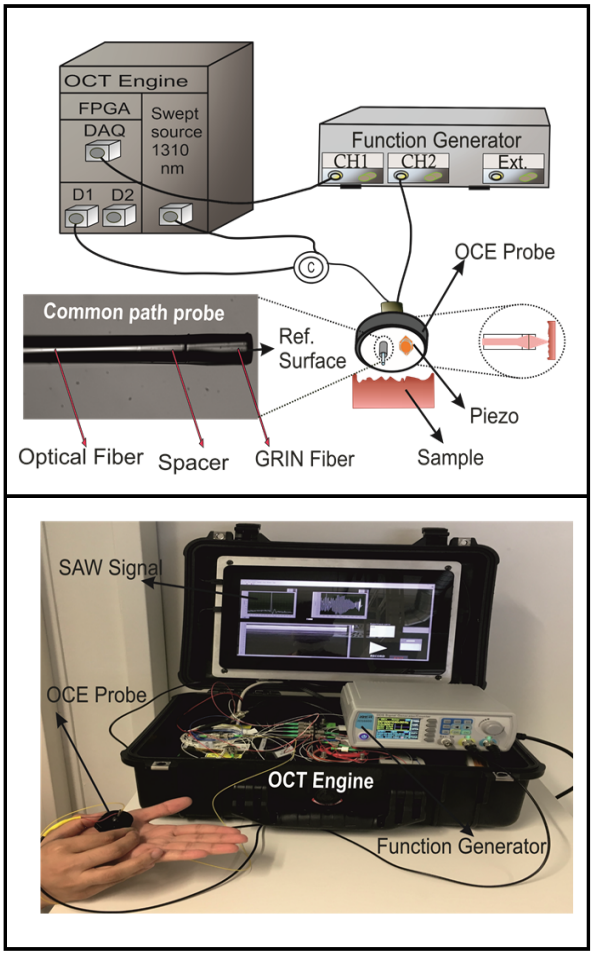

FIGURE 1. (Top) Schematic of the SS-OCEcp system. (Bottom) Picture of the full system placed on a portable cart along with the OCE probe placed on the palm skin.

(Intel NUC Kit NUC8i7HNK Intel Core i7) and a touch screen for display.

The OCE probe is composed of two individual components; a single-mode common path optical fiber assembly for the OCT signal and a piezo transducer for exciting the SAW in the tissue. The OCT part of the OCE probe is based on a common path approach and the schematic of the tip of the fiber is shown in the zoom section of Figure 1 along with the picture of the fiber tip. For the OCT part, the light from the laser source is coupled to the input port of a single-mode fiber (SMF28) based optical circulator (C, CIRC-3-1310, AFW Technologies, Australia). A multimode fiber (FG105LVA, Thorlabs, USA) of length 200 μm and 105 μm core diameter is spliced to the tip of the fiber at the exit port of the circulator. The light exiting the core of the single-mode fiber expands in the multimode fiber section. A 285 μm long GRIN fiber (F-MPD, Newport Corporation, USA) with the core diameter of 100 μm is spliced at the tip of the multimode fiber which focuses the light at a distance of 150 μm approximately from the tip. A part of the illumination is reflected at the tip of the fiber assembly which is used as the reference (Ref.) signal (23 μW) for the OCT and the rest of the light (14 mW) is

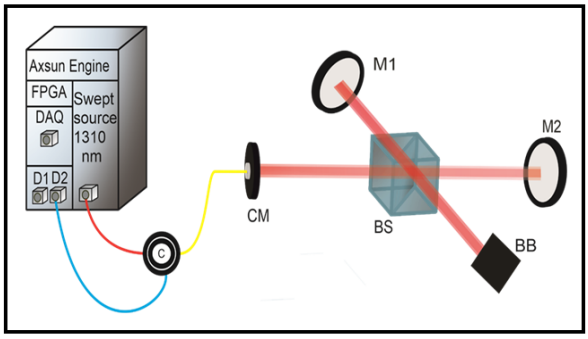

FIGURE 2. Schematic of the SS-OCEncp system. (C) circulator, (CM) collimator, (BS) beam splitter, (M) mirror, (BB) beam block.

focused on the tissue. The reflected light from the tissue is collected back by the fiber assembly and is guided towards the detection photodiode D2 via the circulator. The signal from the photodiode is sent to the integrated data processing unit of the OCT engine.

The piezo unit of the OCE probe consists of a stacked piezo-transducer (PK2FMP2, Thorlabs Inc., USA), capable of producing 11.2 μm displacement at a voltage of 75 volts. A small metallic piece of 1 $\times$ 5 $\times$ 2 mm size is glued at the tip of the piezo such that the 1 $\times$ 5 mm side of the piece faces towards the tissue. The distance between the piezo tip and the fiber tip is measured to be 4.2 mm. When the piezo unit driven by a 0-10 V pulsed voltage signal with 0.1 % duty cycle from a signal generator (National Instruments, USA) at 40 Hz, comes in contact with the tissue, it excites SAW in the tissue which is detected by the OCT part of the system. A TTL signal from the signal generator at 40 Hz and phase-shifted by 180 degrees with respect to the piezo driving signal is used as a trigger for the OCT frame acquisition. This way, the piezo transducer, and the OCT acquisition are synchronized with each other and the SAW appears in the middle of the scan. The whole system was assembled in a portable case (Peli Case 1500) and weighed approximately 8 kilograms.

In Figure 2, we show a non–common path Michelson interferometry-based benchtop system. This system is used to compare the performance of the common path probe-based system with the non-common path-based system. In this design, the input port of a circulator (C) is connected to the light source. The light exiting the output port of the circulator is collimated using a collimator (CM). The collimated light is passed through a non-polarizing beam splitter (BS) to form the reference arm and the sample arm. The light in the reference arm is directed towards a reference mirror (M1) and a sample mirror (M2). The reflected light from both arms is coupled back to the circulator through the collimator and detected using one of the photodiodes (D2).

For both, the common path and the non-common path approach, the data processed by the data processing unit of the OCT engine in the form of A-scan's FFT, is accessed by the host computer via a custom-designed LabVIEW software (National Instruments, USA). From the FFT data, phase and

intensity values are calculated for a full-frame acquired in M-scan mode which is composed of 312 A-scans of the sample at the same location. The number of A-scans was decided by the repetition rate (12.5 kHz) of the swept-source laser. The measured phase values are converted to the displacement of the tissue using the relation

$$\Delta z = \frac{\lambda}{4\pi}\Delta\phi \tag{1}$$

Here Δz is the optical path difference change, λ is the central wavelength of the source, and $\Delta\phi$ is the phase change between adjacent A-Scans.

When the measured displacement of the tissue is plotted against time, it appears as a pulse whose peak position is shifted with respect to the piezo excitation pulse. We measured the displacement of the piezo tip directly using a separate common path patch cable. This provides us the real shape and the position in time for the SAW excitation pulse. The delay between the SAW excitation pulse and the measured tissue displacement pulse is used to calculate the SAW velocity. To achieve this, the distance between the piezo transducer which is measured to be 4.2 mm is divided by the delay between the SAW excitation pulse and the measured tissue displacement pulse.

The resolution with which the velocity of the SAW can be measured depends on the temporal resolution of the system. Our system operates at 12.5 kHz, hence the temporal resolution of the system is 80 μs. This limits the minimum measurable change in the SAW velocity. We improved the temporal resolution of our system by first upsampling the data of the SAW excitation pulse and the tissue displacement pulse by 10 times and then by measuring the peak of the cross-correlation of the two data sets. Using this technique we can precisely measure the position of the SAW peak in the tissue with respect to the SAW excitation pulse at the piezo. For this method, the precision with which the delay between the two pulses can be measured is only limited by the noises present in the system. Finally, the measured SAW velocities are converted to the Young's modulus values using the simplified relation [16]

$$E = 3\rho c_S^2 \tag{2}$$

where tissue is assumed to be incompressible, ρ is the material density and c_S is the SAW velocity in the sample. For soft biological samples such as skin, material density (ρ) = 1060 kg/m^3, can be used [45].

The developed system was tested on agar phantoms and the hand skin of a healthy volunteer. All the methods carried out in this work are in accordance with relevant guidelines and regulations from the local institutional review board (Ethikkommission der Friedrich-Alexander-Universität, Erlangen, Germany). Testing on hand was performed as a self-test on the authors of the manuscript who signed informed consent to participate. No other human experiments were performed in this work.

III. RESULTS

A. DISPLACEMENT STABILITY

To check the phase stability and minimum displacement measurable by our swept-source OCE common path (SS-OCEcp) system, we glued a mirror on the probe holder and measured the displacement of the mirror with respect to the tip of the fiber probe which acts as the reference surface. Since the mirror was fixed to the probe holder, we expect a minimum change in the OPD between the reference signal and the mirror signal. In this case, the measured displacement would represent the noise in the system. For comparison, we also measured the phase stability and minimum displacement measured by a Michelson interferometer-based benchtop non-common path (SS-OCEncp) system under the same standard laboratory conditions as SS-OCEcp measurements. For the SS-OCEncp system, we measured the displacement between two fixed mirrors which were used as reference and sample surfaces in the two arms of the interferometer. Also, since the mirrors were fixed, the measured displacement represents the phase stability of the system which is limited by the mechanical vibration present within the system. In Figure. 3 we show the phase stability of the SS-OCEcp and the SS-OCEncp. In Figure 3(a) and 3(b), we have plotted a part of the interference spectrum of 312 consecutive A-scans for the SS-OCEncp and the SS-OCEcp respectively. The degree of the phase stability of the system is measured by measuring the change in the phase of the fringes between consecutive A-scans. Ideally, if all the consecutive fringes overlap with each other, then the system is considered phase stable. From Figure 3(c), we can see that the phase stability of SS-OCEcp system is much better than the SS-OCEncp system. To quantify the measured values, we calculated the standard deviation of the measured phase values for both systems. The standard deviation of the measured phase change between the reference surface and sample surface for the SS-OCEncp and SS-OCEcp was found to be 952 mrad (99.2 nm displacement) and 98 mrad (10.2 nm displacement) respectively.

B. MEASUREMENT OF MECHANICAL PROPERTIES OF TISSUE PHANTOM

To test the feasibility of the system to measure the mechanical properties of the tissue, we measured the velocity of the SAW generated in agar phantoms using our SS-OCEcp system. The agar phantoms were fabricated by mixing agar powder with a concentration of 1%, 2%, and 3% respectively in water and mixed with few drops of milk to increase the scattering of the light for the SS-OCEcp system. We placed the probe on the phantoms and generated the SAW in the sample using the piezo-transducer. The excitation voltage signal of the piezo-transducer was synchronized with the frame trigger of the OCT system. In Figure 4, we show the measured displacement of the phantom surface for different agar compositions along with a typical M-Scan for the agar phantoms. By monitoring the delay between the excitation

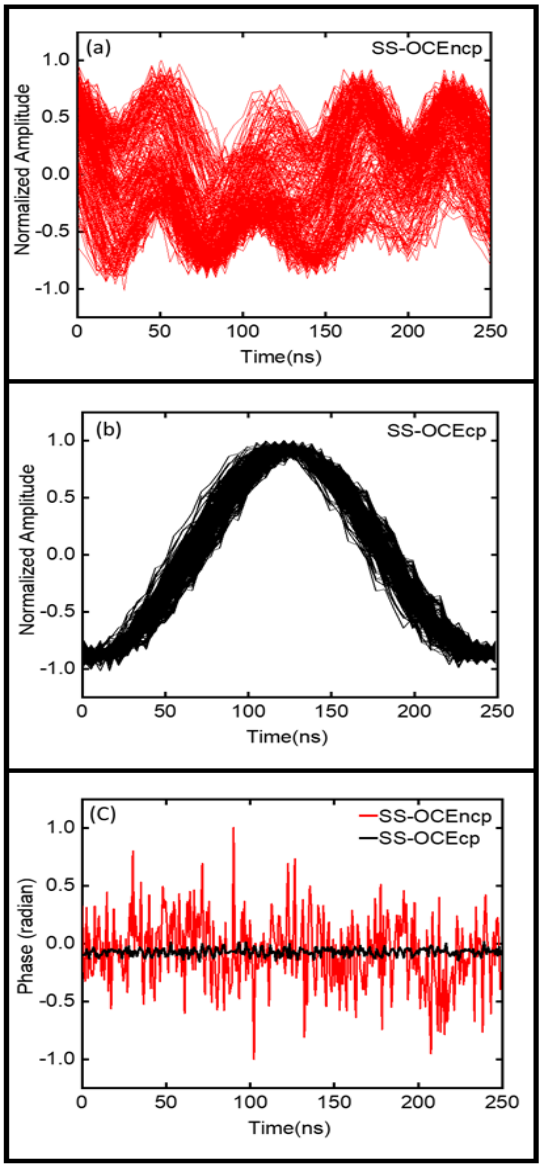

FIGURE 3. Fringe stability for (a) the SS-OCEncp and (b) the SS-OCEcp systems and (c) the measured phase for both systems.

pulse and the SAW peak at the measurement point, we calculated the velocity of the SAW in the sample. For 1%,2%, and 3% agar phantoms, SAW velocity was found to be 5.25 ± 0.03 m/s, 8.75 ± 0.04 m/s, and 10.5 ± 0.06 m/s respectively which corresponds to Young's modulus of 87.64 ± 1.01 kPa, 243.46 ± 2.23 kPa, and 350.59 ± 4.02 kPa respectively. The obtained results from agar phantoms are found to be comparable with previous works [45].

C. MEASUREMENTS OF THE ELASTIC PROPERTIES OF HUMAN SKIN IN-VIVO

To test the performance of the purposed SS-OCEcp system in biological samples, we measured the elastic properties of the human skin in four healthy individuals. In Figure 5, we show the normalized amplitude of the displacement of the skin

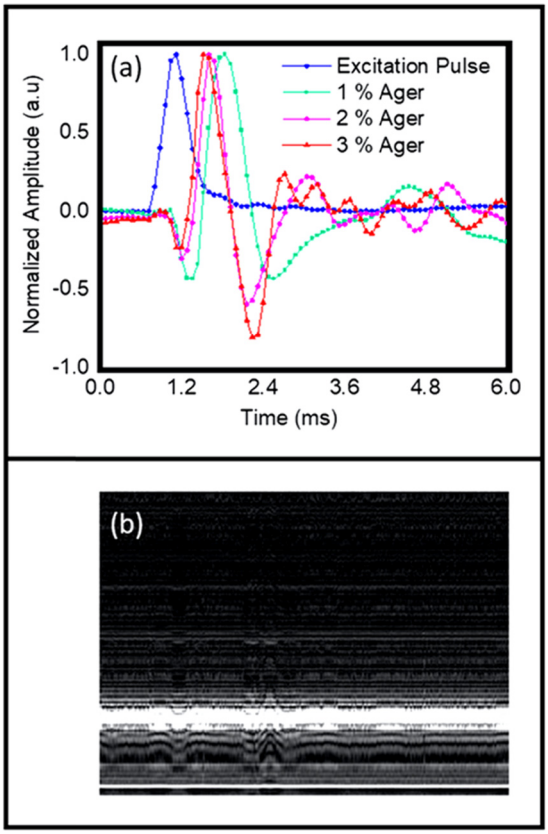

FIGURE 4. (a) Normalized amplitude of the displacement caused by the SAW for different concentrations of the agar phantoms. (b) OCT frame in M-mode for the 3% agar phantom acquired over 25 milliseconds at one location, image size in depth equals 1 mm.

tissue at different locations on hand caused by the SAW for one exemplary healthy individual. The SAW velocity for

the palm (8.52 ± 0.08m/s) was found to be more than the SAW velocity for the forearm (5.09 ± 0.06m/s) which is expected since the palm skin is much stiffer than the forearm skin.

The obtained results for the SAW velocity in human skin are comparable with previous works [42]. In Figure 6, we show the calculated Young's Modulus for all the 4 volunteer measures at palm and forearm skin as a box chart. It can be seen from Figure 6, that the measured values of Young's modulus for palm are much higher than that of forearm skin demonstrating that our system can differentiate between different skin types with different elastic properties.

D. REPEATABILITY MEASUREMENTS FOR THE MECHANICAL PROPERTIES

An important parameter for the clinical systems is the ability to get reliable and repeatable results. For OCE systems, this is primarily limited by the accuracy with which the delay between the SAW at the excitation point and the SAW at the measurement point can be determined. Parameters such as the system's electronic jitter, the bandwidth of the mechanical wave, system stability will limit the delay measurement

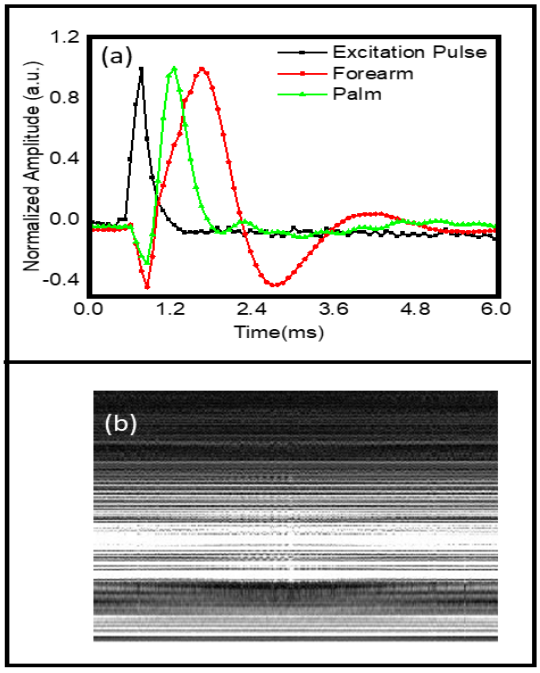

FIGURE 5. (a) Normalized amplitude of the displacement caused by the SAW for different locations on hand. (b) OCT frame in M-mode for the forearm skin acquired over 25 milliseconds at one location, image size in depth equals 1 mm.

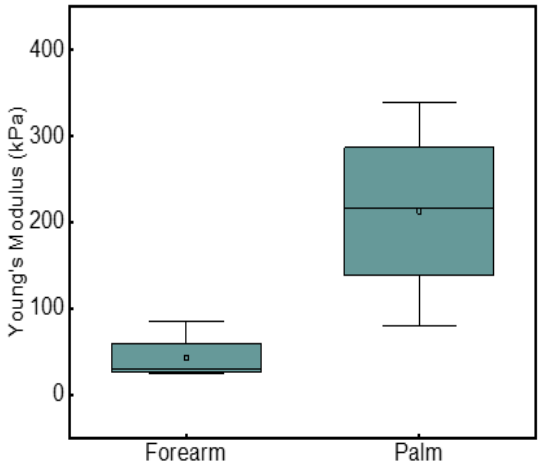

FIGURE 6. Box chart representation of the measured Young's modulus in 4 healthy volunteers for palm and forearm skin.

accuracy. Although the temporal resolution of our system is 80 μs, we can estimate the peak of the SAW with an accuracy of 2.04μs using the upsampled cross-correlation method. This sets the lower limit with which we can accurately measure the time it takes for the SAW to travel from the excitation point to the measurement point. We also performed repeated measurements on agar phantom and human skin with our common path probe to characterize the inter-measurement variability. To quantify the variations within different measurements, we recorded several measurements for SAW time delay, measured at the same location on the sample. Then we measured the variations in the measured values of the SAW time delay for these samples. The standard deviation in the measured SAW time delay for 3% agar phantom and palm skin was found to be 2.42 μs, 2.68 μs respectively.

IV. DISCUSSION

We have developed a system with an SS-OCEcp approach to characterize the mechanical properties of the biological samples. We used a piezo-transducer and single-mode optical fiber-based common path probe to generate and detect surface-induced acoustic waves respectively. By measuring the phase change between the adjacent A-scans, we calculated the displacement of the tissue caused by the SAW. Due to the common path approach, the undesired OPD change between the reference surface and the sample surface was minimized. In comparison to a non-common path approach, the common path approach achieved an order of magnitude better sensitivity in terms of phase or displacement measurement. The developed system allowed to measure extremely small movements (few nanometers) inside the tissue which were caused by the SAW. A measurement of the delay between the SAW at the excitation point and the measurement point allowed us to calculate the velocity of the SAW in the sample which represents the mechanical properties of the sample. We tested the developed system using tissue phantoms made of agar which is known to possess mechanical properties similar to soft biological tissue. We also measured the mechanical properties of skin at different locations on hand and the measured values were found to be similar to the previously reported values.

One of the limitations of our current system is that we have performed measurements at a single tissue location. Previously, several studies have measured the mechanical properties of the tissue at multiple points along the SAW propagation path. Multiple point measurement allows measuring the dispersion in the SAW as the waves propagate within and on the surface of the sample. Dispersion of SAW can be used to calculate the depth-dependent mechanical properties of the sample as low frequencies represent properties of the deep tissue and higher frequencies represent more of the surface properties [46]. This however should not be seen as a limitation of the system as it allows to greatly simplify the probe design which is highly desired for clinical settings. Nevertheless, non-scanning (single point measurement) systems have been extensively used in previous studies to determine the mechanical properties of the tissue and our common path approach along with the portable system will add immensely to such studies.

In our system, we have used a swept-source laser which usually suffers from poor phase stability [47]. The phase stability of a swept-source system can be improved using fiber Bragg grating [48]. The displacement measurement sensitivity of the common path approach can be further improved using light sources such as superluminescent diodes. However, it should be noted that such sources can only be used for spectrometer-based OCT systems which suffer from degraded signal to noise ratio as the sample signal moves

away from the zero optical path difference with respect to the reference surface.

From a clinical point of view, it might be more desirable to use a non-contact approach to excite SAW in the sample whereas in our current system we have used a piezo actuator for this purpose. Our common path OCE probe can be combined with air puff or nano second laser excitation schemes to develop a non-contact OCE system. Nevertheless, our current approach demonstrates the superior performance of common path OCE probes compared to the non-common path systems. The portable OCE system and the handheld probe with improved phase measurement sensitivity make an ideal combination for a clinical system that can be used to measure the mechanical properties of the tissue in vivo.

REFERENCES

[1] C. Alibert, B. Goud, and J.-B. Manneville, "Are cancer cells really softer than normal cells?" *Biol. Cell*, vol. 109, no. 5, pp. 167–189, May 2017.

[2] B. S. Garra, E. I. Cespedes, J. Ophir, S. R. Spratt, R. A. Zuurbier, C. M. Magnant, and M. F. Pennanen, "Elastography of breast lesions: Initial clinical results," *Radiology*, vol. 202, no. 1, pp. 79–86, Jan. 1997.

[3] E. V. Gubarkova, A. A. Sovetsky, V. Y. Zaitsev, L. A. Matveev, A. L. Matveyev, D. A. Vorontsov, A. A. Plekhanov, S. S. Kuznetsov, M. A. Sirotkina, A. Y. Vorontsov, and N. D. Gladkova, "Assessment of human breast cancer margins by compressional optical coherence elastography," *Proc. SPIE*, vol. 11457, Apr. 2020, Art. no. 1145709.

[4] A. Balbir-Gurman, C. P. Denton, B. Nichols, C. J. Knight, A. M. Nahir, G. Martin, and C. M. Black, "Non-invasive measurement of biomechanical skin properties in systemic sclerosis," *Ann. Rheumatic Diseases*, vol. 61, no. 3, pp. 237–241, 2002.

[5] D. N. H. Enomoto, J. R. Mekkes, P. M. M. Bossuyt, R. Hoekzema, and J. D. Bos, "Quantification of cutaneous sclerosis with a skin elasticity meter in patients with generalized scleroderma," *J. Amer. Acad. Dermatol.*, vol. 35, no. 3, pp. 381–387, Sep. 1996.

[6] C. Liu, S. Assassi, S. Theodore, C. Smith, A. Schill, M. Singh, S. Aglyamov, C. Mohan, and K. V. Larin, "Translational optical coherence elastography for assessment of systemic sclerosis," *J. Biophoton.*, vol. 12, no. 12, Dec. 2019, Art. no. e201900236.

[7] G. Kumánovics, M. Péntek, S. Bae, D. Opris, D. Khanna, D. E. Furst, and L. Czirják, "Assessment of skin involvement in systemic sclerosis," *Rheumatology*, vol. 56, pp. V53–V66, Sep. 2017.

[8] R. Kamp, A. Möltner, and S. Harendza, "'Princess and the pea'—An assessment tool for palpation skills in postgraduate education," *BMC Med. Educ.*, vol. 19, no. 1, p. 177, May 2019.

[9] Q. S. Li, G. Y. H. Lee, C. N. Ong, and C. T. Lim, "AFM indentation study of breast cancer cells," *Biochem. Biophys. Res. Commun.*, vol. 374, no. 4, pp. 609–613, Oct. 2008.

[10] Z. Zhou, C. Zheng, S. Li, X. Zhou, Z. Liu, Q. He, N. Zhang, A. Ngan, B. Tang, and A. Wang, "AFM nanoindentation detection of the elastic modulus of tongue squamous carcinoma cells with different metastatic potentials," *Nanomed., Nanotechnol., Biol. Med.*, vol. 9, no. 7, pp. 864–874, Oct. 2013.

[11] J. Rother, H. Nöding, I. Mey, and A. Janshoff, "Atomic force microscopy-based microrheology reveals significant differences in the viscoelastic response between malign and benign cell lines," *Open Biol.*, vol. 4, no. 5, May 2014, Art. no. 140046.

[12] Y. K. Mariappan, K. J. Glaser, and R. L. Ehman, "Magnetic resonance elastography: A review," *Clin. Anatomy*, vol. 23, pp. 497–511, Jul. 2010.

[13] J.-L. Gennisson, T. Deffieux, M. Fink, and M. Tanter, "Ultrasound elastography: Principles and techniques," *Diagnostic Intervent. Imag.*, vol. 94, no. 5, pp. 487–495, May 2013.

[14] G. Scarcelli and S. H. Yun, "Confocal Brillouin microscopy for three-dimensional mechanical imaging," *Nature Photon.*, vol. 2, no. 1, pp. 39–43, Jan. 2008.

[15] B. F. Kennedy, K. M. Kennedy, and D. D. Sampson, "A review of optical coherence elastography: Fundamentals, techniques and prospects," *IEEE J. Sel. Topics Quantum Electron.*, vol. 20, no. 2, pp. 272–288, Mar. 2014.

[16] K. V. Larin and D. D. Sampson, "Optical coherence elastography–OCT at work in tissue biomechanics [Invited]," *Biomed. Opt. Exp.*, vol. 8, no. 2, pp. 1172–1202, Feb. 2017.

[17] C. W. Ballmann, J. V. Thompson, A. J. Traverso, Z. Meng, M. O. Scully, and V. V. Yakovlev, "Stimulated Brillouin scattering microscopic imaging," *Sci. Rep.*, vol. 5, no. 1, Nov. 2016, Art. no. 018139.

[18] L. M. Sakata, J. DeLeon-Ortega, V. Sakata, and C. A. Girkin, "Optical coherence tomography of the retina and optic nerve—A review," *Clin. Experim. Ophthalmol.*, vol. 37, no. 1, pp. 90–99, Jan. 2009.

[19] J. Olsen, J. Holmes, and G. B. Jemec, "Advances in optical coherence tomography in dermatology—A review," *J. Biomed. Opt.*, vol. 23, pp. 1–10, Apr. 2018.

[20] J. Wang, Y. Xu, and S. A. Boppart, "Review of optical coherence tomography in oncology," *J. Biomed. Opt.*, vol. 22, pp. 1–23, Dec. 2017.

[21] H. G. Bezerra, M. A. Costa, G. Guagliumi, A. M. Rollins, and D. I. Simon, "Intracoronary optical coherence tomography: A comprehensive review: Clinical and research applications," *JACC, Cardiovascular Intervent.*, vol. 2, no. 11, pp. 1035–1046, Nov. 2009.

[22] W. Tan, A. L. Oldenburg, J. J. Norman, T. A. Desai, and S. A. Boppart, "Optical coherence tomography of cell dynamics in three-dimensional tissue models," *Opt. Exp.*, vol. 14, pp. 16, pp. 7159–7171, Aug. 2006.

[23] S. Takarada, T. Imanishi, Y. Liu, H. Ikejima, H. Tsujioka, A. Kuroi, K. Ishibashi, K. Komukai, T. Tanimoto, Y. Ino, H. Kitabata, T. Kubo, N. Nakamura, K. Hirata, A. Tanaka, M. Mizukoshi, and T. Akasaka, "Advantage of next-generation frequency-domain optical coherence tomography compared with conventional time-domain system in the assessment of coronary lesion," *Catheterization Cardiovascular Intervent.*, vol. 75, no. 2, pp. 202–206, Feb. 2010.

[24] K. M. Tan, M. Mazilu, T. H. Chow, W. M. Lee, K. Taguchi, B. K. Ng, W. Sibbett, C. S. Herrington, C. T. A. Brown, and K. Dholakia, "In-fiber common-path optical coherence tomography using a conical-tip fiber," *Opt. Exp.*, vol. 17, no. 4, pp. 2375–2384, 2009.

[25] U. Sharma, N. M. Fried, and J. U. Kang, "All-fiber common-path optical coherence tomography: Sensitivity optimization and system analysis," *IEEE J. Sel. Topics Quantum Electron.*, vol. 11, no. 4, pp. 799–805, Jul. 2005.

[26] Y. Huang, X. Liu, C. Song, and J. U. Kang, "Motion-compensated hand-held common-path Fourier-domain optical coherence tomography probe for image-guided intervention," *Biomed. Opt. Exp.*, vol. 3, no. 12, pp. 3105–3118, 2012.

[27] K. Singh, D. Yamada, and G. Tearney, "Common path side viewing monolithic ball lens probe for optical coherence tomography," *Sovremennye Tehnologii Med.*, vol. 7, no. 1, pp. 29–33, Mar. 2015.

[28] K. Singh, R. Reddy, G. Sharma, Y. Verma, J. A. Gardecki, and G. Tearney, "In-line optical fiber metallic mirror reflector for monolithic common path optical coherence tomography probes," *Lasers Surgery Med.*, vol. 50, no. 3, pp. 230–235, Mar. 2018.

[29] K. Blessing, S. Sharma, A. Gumann, and K. Singh, "Low cost scalable monolithic common path probe design for the application in endoscopic optical coherence tomography," *Eng. Res. Exp.*, vol. 1, no. 2, Oct. 2019, Art. no. 025008.

[30] T. Marvdashti, L. Duan, K. L. Lurie, G. T. Smith, and A. K. Ellerbee, "Quantitative measurements of strain and birefringence with common-path polarization-sensitive optical coherence tomography," *Opt. Lett.*, vol. 39, no. 19, pp. 5507–5510, 2014.

[31] J.-U. Kang, J.-H. Han, X. Liu, and K. Zhang, "Common-path optical coherence tomography for biomedical imaging and sensing," *J. Opt. Soc. Korea*, vol. 14, no. 1, pp. 1–13, Mar. 2010.

[32] J. U. Kang, J.-H. Han, X. Liu, K. Zhang, C. G. Song, and P. Gehlbach, "Endoscopic functional Fourier domain common-path optical coherence tomography for microsurgery," *IEEE J. Sel. Topics Quantum Electron.*, vol. 16, no. 4, pp. 781–792, Jul. 2010.

[33] A. V. Maslennikova, M. A. Sirotkina, A. A. Moiseev, E. S. Finagina, S. Y. Ksenofontov, G. V. Gelikonov, L. A. Matveev, E. B. Kiseleva, V. Y. Zaitsev, E. V. Zagaynova, F. I. Feldchtein, N. D. Gladkova, and A. Vitkin, "*In-vivo* longitudinal imaging of microvascular changes in irradiated oral mucosa of radiotherapy cancer patients using optical coherence tomography," *Sci. Rep.*, vol. 7, no. 1, p. 16505, Dec. 2017.

[34] A. Moiseev, S. Ksenofontov, M. Sirotkina, E. Kiseleva, M. Gorozhantseva, N. Shakhova, L. Matveev, V. Zaitsev, A. Matveyev, E. Zagaynova, V. Gelikonov, N. Gladkova, A. Vitkin, and G. Gelikonov, "Optical coherence tomography-based angiography device with real-time angiography B-scans visualization and hand-held probe for everyday clinical use," *J. Biophoton.*, vol. 11, no. 10, Oct. 2018, Art. no. e201700292.

[35] D. Zhang, J. Wang, C. Li, and Z. Huang, "Optimal stimulation frequency for vibrational optical coherence elastography," *J. Biophoton.*, vol. 13, no. 2, Feb. 2020, Art. no. e201960066.
[36] G. Lan, M. Singh, K. V. Larin, and M. D. Twa, "Common-path phase-sensitive optical coherence tomography provides enhanced phase stability and detection sensitivity for dynamic elastography," *Biomed. Opt. Exp.*, vol. 8, no. 11, pp. 5253–5266, 2017.
[37] Y. Li, S. Moon, J. J. Chen, Z. Zhu, and Z. Chen, "Ultrahigh-sensitive optical coherence elastography," *Light, Sci. Appl.*, vol. 9, no. 1, p. 58, Dec. 2020.
[38] K. M. Kennedy, B. F. Kennedy, R. A. McLaughlin, and D. D. Sampson, "Needle optical coherence elastography for tissue boundary detection," *Opt. Lett.*, vol. 37, no. 12, pp. 2310–2312, 2012.
[39] K. M. Kennedy, R. A. McLaughlin, B. F. Kennedy, A. Tien, B. Latham, C. M. Saunders, and D. D. Sampson, "Needle optical coherence elastography for the measurement of microscale mechanical contrast deep within human breast tissues," *J. Biomed. Opt.*, vol. 18, no. 12, Dec. 2013, Art. no. 121510.
[40] Y. Qiu, Y. Wang, Y. Xu, N. Chandra, J. Haorah, B. Hubbi, B. J. Pfister, and X. Liu, "Quantitative optical coherence elastography based on fiber-optic probe for in situ measurement of tissue mechanical properties," *Biomed. Opt. Exp.*, vol. 7, no. 2, pp. 688–700, 2016.
[41] R. W. Sanderson, A. Curatolo, P. Wijesinghe, L. Chin, and B. F. Kennedy, "Finger-mounted quantitative micro-elastography," *Biomed. Opt. Exp.*, vol. 10, no. 4, pp. 1760–1773, 2019.
[42] C. Li, G. Guan, R. Reif, Z. Huang, and R. K. Wang, "Determining elastic properties of skin by measuring surface waves from an impulse mechanical stimulus using phase-sensitive optical coherence tomography," *J. Roy. Soc. Interface*, vol. 9, no. 70, pp. 831–841, May 2012.
[43] S. Wang and K. V. Larin, "Noncontact depth-resolved micro-scale optical coherence elastography of the cornea," *Biomed. Opt. Exp.*, vol. 5, no. 11, pp. 3807–3821, 2014.
[44] Y. Qu, T. Ma, Y. He, J. Zhu, C. Dai, M. Yu, S. Huang, F. Lu, K. K. Shung, Q. Zhou, and Z. Chen, "Acoustic radiation force optical coherence elastography of corneal tissue," *IEEE J. Sel. Topics Quantum Electron.*, vol. 22, no. 3, pp. 288–294, May 2016.
[45] C. Li, G. Guan, X. Cheng, Z. Huang, and R. K. Wang, "Quantitative elastography provided by surface acoustic waves measured by phase-sensitive optical coherence tomography," *Opt. Lett.*, vol. 37, no. 4, pp. 722–724, Feb. 2012.
[46] S. Wang and K. V. Larin, "Optical coherence elastography for tissue characterization: A review," *J. Biophoton.*, vol. 8, no. 4, pp. 279–302, Apr. 2015.
[47] S. Song, W. Wei, B.-Y. Hsieh, I. Pelivanov, T. T. Shen, M. O'Donnell, and R. K. Wang, "Strategies to improve phase-stability of ultrafast swept source optical coherence tomography for single shot imaging of transient mechanical waves at 16 kHz frame rate," *Appl. Phys. Lett.*, vol. 108, no. 19, May 2016, Art. no. 191104.
[48] R. K. Manapuram, V. G. R. Manne, and K. V. Larin, "Development of phase-stabilized swept-source OCT for the ultrasensitive quantification of microbubbles," *Laser Phys.*, vol. 18, no. 9, pp. 1080–1086, Sep. 2008.

ASHA PARMAR received the master's degree from Maharshi Dayanand University, Rohtak, India. She is currently pursuing the Ph.D. degree with the Max Planck Institute for the Science of Light, Erlangen, Germany.

GARGI SHARMA received the Ph.D. degree from INRS, Canada, in 2013. She was a Postdoctoral Fellow at the Harvard Medical School, USA, until 2018. She is currently a Postdoctoral Fellow with the Max Planck Institute for the Physics of Light, Germany. Her current research focuses on the development of novel miniaturized devices for optical coherence tomography and thermographic imaging.

SHIVANI SHARMA is currently pursuing the master's degree in physics with Friedrich-Alexander-Universität Erlangen-Nürnberg.

KANWARPAL SINGH received the Ph.D. degree from INRS, Canada, in 2013. He was a Postdoctoral Fellow at the Harvard Medical School, USA, until 2018, where he worked on the development of high-resolution optical coherence tomography systems. He currently leads an independent research group (Microendoscopy) at the Max Planck Institute for the Science of Light, Germany. His research group focuses on the development of miniaturized flexible endoscopic devices for imaging inside the body.